ACADEMIC PRESS

Available online at www.sciencedirect.com
SCIENCE DIRECT®

Journal of Catalysis 217 (2003) 298–309

JOURNAL OF CATALYSIS

www.elsevier.com/locate/jcat

A priori selection of shape-selective zeolite catalysts for the synthesis of 2,6-dimethylnaphthalene

Roberto Millini,* Francesco Frigerio, Giuseppe Bellussi, Giannino Pazzuconi, Carlo Perego, Paolo Pollesel, and Ugo Romano

Physical Chemistry Department, EniTecnologie S.p.A., Via F. Maritano, 26, I-20097 San Donato Milanese, MI Italy

Received 18 September 2002; revised 21 January 2003; accepted 17 February 2003

Abstract

Modeling tools based on molecular mechanics and molecular dynamics were used for selecting shape-selective zeolite catalysts for the synthesis of 2,6-dimethylnapthalene (2,6-DMN) through the alkylation of naphthalene (NAPH) or via isomerization of other DMN isomers. A number of *medium*- (MFI and EUO) and *large-pore* zeolites (*BEA, MOR, MAZ, FAU, LTL, OFF, and MTW) were considered and for each of them the minimum energy pathways for the diffusion of naphthalene, 1- and 2-methylnapthalene (MNs), and 1,5-, 1,6-, 2,6-, and 2,7-dimethylnapthalene (DMNs) were computed. The results of the simulations indicated that the diffusion of MNs and DMNs isomers in the *medium-pore* zeolites is impeded by high-energy barriers, leading to the conclusion that this kind of structure can be used neither in the isomerization nor in the alkylation reaction. In contrast, *large-pore* zeolites are more promising though their behavior strongly depends on the effective size of the pore openings. Among them, MTW was predicted to be the most promising candidate for the selective alkylation of NAPH to 2,6-DMN. In fact, the simulations indicated high-energy diffusion barriers not only for molecules bearing a $-CH_3$ group in the α-position but also for the undesired 2,7-DMN molecule. Catalytic tests, performed in the presence of 1,2,4-trimethylbenzene as a solvent, confirmed the prediction since MTW gave the highest 2,6-DMN yields with a 2,6-/2,7-DMN ratio in the range 2.0–2.6, well above the thermodynamic value of ≈ 1 obtained with the other zeolites. The good catalytic performances of MTW were explained by the fact that, unique among the *large-pore* zeolites considered, this zeolite showed a better stabilization of the 1,1-diarylmethane intermediate molecules leading to 2-MN, 2,6-DMN, and 2,7-DMN. Their formation can be considered more probable than for those deriving from the electrophilic attack of the benzyl carbocation in the α-position of the naphthalene ring.

Keywords: 2,6-Dimethylnaphthalene; Molecular modeling; Diffusion; MTW; Alkylation; Isomerization

1. Introduction

2,6-Dialkylnaphthalenes (2,6-DKN) are key intermediates in the synthesis of polyethylene naphthalate (PEN) which, compared with other thermoplastic polyesters (e.g., polyethylene terephthalate, PET), has improved thermal, mechanical, and gas barrier properties that render it suitable to several applications. The most important synthesis routes to PEN involve the oxidation of 2,6-DKN to the corresponding dicarboxylic acid (2,6-NDA), its esterification with methanol to dimethyl-2,6-naphthalenedicarboxylate (2,6-NDC), and the co-polymerization with ethyleneglycol (Fig. 1). For economical reasons, 2,6-dimethylnaphthalene (2,6-DMN) is preferred to other dialkylnaphthalenes (i.e., 2,6-diethyl- (2,6-DEN) or 2,6-diisopropylnaphthalene (2,6-DIPN)) because no C atoms are lost in the oxidation step; however, its high cost and low availability limit the large-scale production and commercialization of PEN.

To date, 2,6-DMN is produced at large scale (30 kton/year) only by BP-Amoco. The employed process is quite complex, since it involves four subsequent reaction steps: the *o*-xylene/butadiene condensation to 5-*o*-tolylpentene (5-OTP) in the presence of the strongly basic liquid catalyst Na/K, the cyclization of 5-OTP to 1,5-dimethyltetraline (1,5-DMT), and its dehydrogenation to 1,5-dimethylnaphathelene (1,5-DMN), which is finally isomerized to 2,6-DMN [1]. Though complex, this process is economically more favorable with respect to other similar synthesis routes such as those proposed by the Mitsubishi Gas Chemical

* Corresponding author.
E-mail address: rmillini@enitecnologie.eni.it (R. Millini).

0021-9517/03/$ – see front matter
doi:10.1016/S0021-9517(03)00071-X

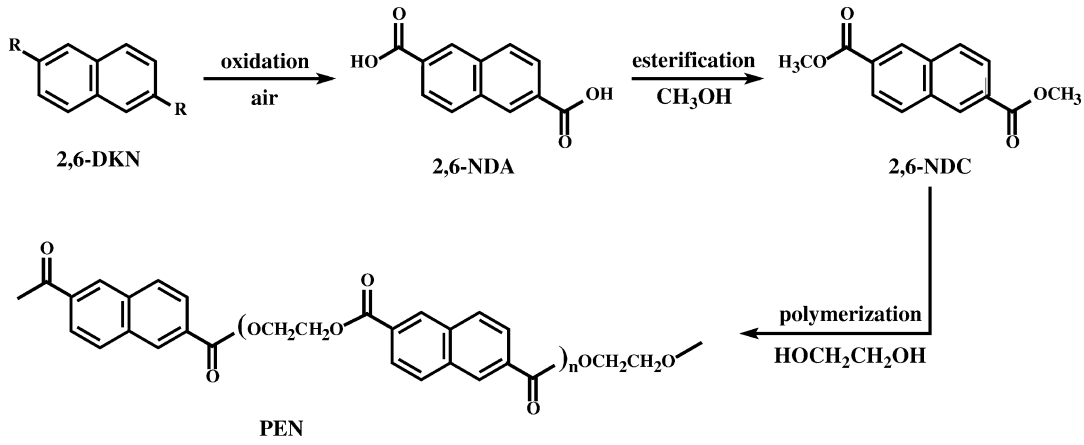

Fig. 1. Synthesis of PEN.

(MGC), based either on toluene, 1-butene, and CO [2] or *m*-xylene, propylene, and CO [3]. Another disadvantage of such processes resides in the catalyst used ($HF \cdot BF_3$), which is seen with environmental concern.

Alternative processes for the synthesis of 2,6-DMN have also been proposed. Mitsui claimed a process based on the preparation of 3-methyl-4-(*p*-tolyl)butane or butene by condensation of *p*-xylene with 1-butene or butadiene in the presence of a supported Na/K catalyst [4]. The successive dehydrocyclization on chromia/alumina, rhenia/alumina, or chromia/rhenia/alumina catalysts gives 2,6-DMN in low yields (25–30%) from the butane intermediate and in high yields (70%) from the butene intermediate [4]. This process was recently improved by Optatech Corp., which proposed new catalysts for both the condensation and the dehydrocyclization reaction [5].

Other simpler and more desirable synthesis routes for obtaining 2,6-DMN involve the methylation of naphthalene (NAPH) or methylnaphthalenes (MNs) in the presence of zeolite catalysts. Different approaches can be used, including the direct alkylation with methanol (with or without paraffinic or aromatic solvents) and the disproportionation of MNs in the presence of various zeolite catalysts including ZSM-5 (MFI), ZSM-11 (MFI/MEL), ZSM-12 (MTW), mordenite (MOR), Y (FAU), FAU/EMT, Beta, MCM-22 (MWW), and NU-87 (NES) [6–16].

From the industrial point of view, two processes have to be mentioned. In 1992, Teijin claimed a two-step process in which NAPH is first reacted with an isomeric DMN mixture to produce MNs; at the same time, isomerization of DMNs occurs to increase the amount of 2,6-DMN. Subsequently, MNs are methylated with methanol to give a 2,6-DMN enriched product [17]. The critical points of this process are the low yields and the consequent high costs due to the extensive recycling involved.

More promising results were jointly claimed by Mobil Technology Company and Kobe Steel [18], who developed a process combining the Mobil's synthesis technology, based on the use of MCM-22 catalyst [19] with the Kobe's separation technology. This process gives good results when 2-MN is used as a single feedstock since the 2,6-/2,7-DMN ratio in the product is 2.3, well above the value (≈ 1.0) predicted from thermodynamic data [12,16]. However, when a mixture of the two MN isomers is fed, the 2,6-/2,7-DMN ratio drops down to 1.2–1.5 [18] and this is a strong limit since the separation of these DMNs is not easy. It cannot be performed by distillation because the difference between their boiling points is 0.3 °C, while by crystallization they form eutectic crystals with a 2,6-/2,7-DMN ratio of 0.7. Therefore, one main goal is to find an efficient process able to produce 2,6-DMN in high yields and with DMN isomers distribution far from the equilibrium.

Recently, we faced this problem by examining the catalytic performances of several zeolite catalysts in the methylation of NAPH and MNs both in the presence and in the absence of solvent [20]. In the latter case, no significant differences from the literature data were observed, while a great improvement in 2,6-DMN selectivity, 2,6-/2,7-DMN ratio, and catalyst life was achieved when 1,2,4-trimethylbenzene (pseudocumene, TMB) was used as a solvent. The adopted reaction conditions allowed transmethylation and the zeolite catalyst was ZSM-12 [21].

The catalyst screening was preceded by a molecular modeling study based on the use of molecular mechanics and dynamics calculations, with the aim of providing information about the most promising zeolite structures potentially able to increase the 2,6-DMN selectivity. In the past decade, the development of efficient modeling tools expressly dedicated to the study of heterogeneous catalysts improved the capabilities of understanding their structure–property relationships at a molecular level. For porous catalysts, great advantages derived from the application of methods based on molecular mechanics (MM) and dynamics (MD) that were developed for evaluating the shape-selectivity properties of zeolite structures in a given reaction. In particular, in a microporous solid the overall process can be regarded as the sum of three different main steps: (1) the adsorption and diffusion of reactant(s); (2) the reaction; and (3) the diffusion and desorption of product(s).

The diffusion of the different species (reactant(s) and product(s)) involved in the reaction can be efficiently simulated in large systems by using classical MM and MD approaches, providing useful indications about the reactant and product shape-selectivity properties of different microporous structures. Horsley et al. were the first to perform a computer-assisted screening of zeolite catalysts and, curiously enough, the problem they faced is similar to that under our investigation, i.e., the selection of a catalyst for the selective isopropylation of NAPH to 2,6-DIPN [22]. This method was further applied to the interpretation of the results obtained from various catalytic tests: e.g., the skeletal isomerization of 1-butene to isobutene [23,24], the alkylation of benzene with propylene to cumene [25], the hydroconversion of *n*-heptane [26], and the study of the alkylbenzene diffusion in *large-pore* zeolites [27].

The reaction mechanism modeling (step 2) actually requires the use of computationally demanding quantum mechanical (QM) methods, which for that reason are usually applied to small clusters, not representative of the overall structure. Therefore, QM methods can hardly be applied to study the reaction mechanism on different zeolite structures, even if the recently developed embedded-type approaches are described as very promising tools [28]. However, when the reaction mechanism is known, indirect information can be obtained by evaluating the interactions of molecules, representative of the transition states or of the intermediates, with different microporous frameworks. For example, Raybaud et al. compared the computed adsorption enthalpies of five cyclopropane molecules, representative of the corresponding protonated intermediates involved in the hydroisomerization of *n*-heptane, in the ZSM-22 (TON), EU-1 (EUO), and Beta zeolites [26]. In this way, the authors concluded that only ZSM-22 imposes steric control of the reaction pathway [26].

In this paper we report the results of the computational study aimed at screening potential zeolite catalysts for the synthesis of 2,6-DMN. The predictions of the modeling study are compared to the results of the catalytic tests reported in [20].

2. Definition of the problem

2.1. Isomerization of DMNs

A mixture of DMNs may contain 10 different isomers, which are difficult to separate. From the thermodynamic point of view, the β-position is preferred with respect to the α-, as demonstrated by the isomers distribution at the thermodynamic equilibrium computed at 400 °C (Table 1) [12,16]. It was demonstrated that the DMN isomers can be divided into the following groups:

(A) 1,5-DMN; 1,6-DMN; 2,6-DMN
(B) 1,8-DMN; 1,7-DMN; 2,7-DNM

Table 1
Calculated DMN isomers distribution at the thermodynamic equilibrium at 400 °C

Isomer	Ref. [12]	Ref. [16]
1,7-DMN	14.7	15.8
2,7-DMN	11.7	12.7
1,3-DMN	14.8	16.0
2,6-DMN	12.0	12.8
1,6-DMN	14.0	12.8
1,4-DMN	5.0	4.8
1,5-DMN	6.0	5.9
2,3-DMN	12.1	11.8
1,2-DMN	9.7	7.4
1,8-DMN	0.0	0.0

(C) 1,4-DMN; 1,3-DMN; 2,3-DMN
(D) 1,2-DMN

and the isomerization was considered to occur within each group [13]. That means that the shift of a $-CH_3$ group from the α-position to the β-position in the same ring is easy, while from the β-position to the β-position or from a ring to another is rather difficult [13]. Therefore, only isomers belonging to group A are considered of interest. If this reaction is to be performed in a microporous catalyst, pores large enough to allow the adsorption and diffusion of the most hindered 1,5-DMN isomer should characterize the selected zeolite. In this case, the reaction does not proceed under steric control while on the other hand the acidic properties of the catalyst should be most effective.

2.2. 2,6-DMN from the alkylation of NAPH and MN in the presence of TMB

As far as the alkylation reaction of NAPH and MN is concerned, the goal is to identify zeolite catalysts, which can favor the formation of 2,6-DMN with high selectivity while limiting the formation of the other isomers. Therefore, a suitable zeolite catalyst should allow the diffusion of the reagents and of the 2,6-DMN but not that of the other isomers with a $-CH_3$ group in the α-position. Consequently these undesired products should undergo isomerization to less hindered species, before elution. Another important point concerns the 2,7-DMN isomer, which can be easily formed but cannot undergo easy isomerization to the desired product (see above). The formation of this isomer should be avoided because of its difficult separation from 2,6-DMN (see Introduction). A similar problem was faced by Horsley et al. when they studied the alkylation reaction of NAPH with isopropanol to 2,6-DIPN [22]. In the present case, the problem is much more intriguing because of the significantly lower steric hindrance of the methyl group with respect to the isopropyl one. From the thermodynamic point of view, the 2,6- and 2,7-DMN isomers are equally favored; hence, the formation of the undesired product should be limited by accurately exploiting the *shape-selectivity* property of zeolite catalysts.

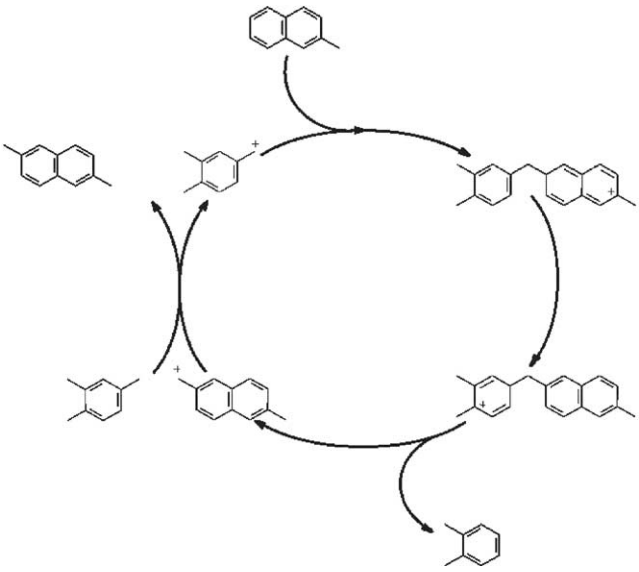

Fig. 2. Proposed mechanism of methylation of 2-MN with TMB.

When the reaction is performed in the presence of TMB as a solvent, the formation of the products occurs via transmethylation between TMB and NAPH or MNs [20]; the bimolecular reaction mechanism involves the electrophilic attack of a benzyl carbocation to the aromatic ring, with the formation of a 1,1-diarylmethane intermediate [29] (Fig. 2). Therefore, another interesting point to exploit is the zeolite inhibition of the formation of intermediates deriving from the attack of the benzyl cation to the α-position of the naphthalene ring. Accordingly, an accurate evaluation is required of the location and energetics of the model molecules derived from the possible intermediates.

3. Methodology

3.1. Determination of the energy barriers to molecular diffusion

The procedure, first proposed by Horsley et al. [22], is based on the determination of the minimum energy pathway (MEP) of a *guest* molecule in a given *host* framework as exemplified in Fig. 3. With this procedure, a zeolite model is first built and the initial pathway is assumed to be a straight line connecting to dummy atoms A and B (with null potential) located at the center of the pore openings at the opposite ends of the zeolite model (Fig. 3). Chosen a pivot atom P, the simulation is performed by applying successive translations Δx (in these cases 0.2 Å long) along the defined path while a strong harmonic potential constrains the atom P to lie on a plane perpendicular to the $A \rightarrow B$ direction and located at a fixed distance from the two dummy atoms. After each translation, the energy of the molecule is minimized with respect to its internal degrees of freedom (i.e., bond lengths, bond angles, torsion angles, out-of-plane deformation, etc.) as well as to the nonbonded interactions with the framework atoms (computed with the classical Lennard-Jones 9-6 potential energy function), while the zeolite model is kept fixed. Once minimized, the molecule is moved to the next position and further minimized and the whole process is iterated until the end of the path is reached. The result of the calculation is the minimum energy profile along the diffusion pathway from which the energy barriers for diffusion can be estimated.

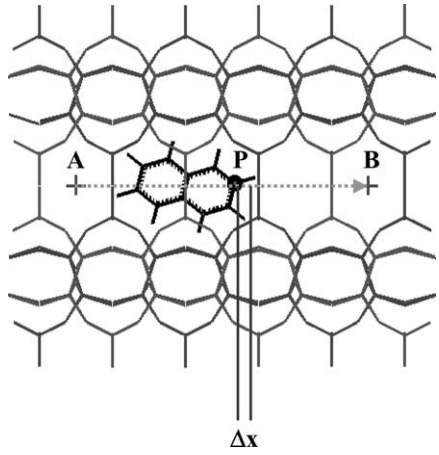

Fig. 3. Procedure for the determination of the minimum energy pathway (MEP). A and B are the two dummy atoms defining the initial pathway; P is the pivot atom constrained to lie in a plane perpendicular to the initial pathway; Δx is the motion step (0.2 Å long in this work).

The zeolite models were built with the Solids_Builder module of MSI Catalysis software package (release 7.0) [30]. The model dimensions were chosen to allow the *guest* molecule to move along a path 25–40 Å long (with a number of framework atoms in the range 900–1700). Energy minimization was performed with Discover [31] using the *cvff_91czeo* force field [32], which is based on the consistent valence force field (*cvff*) [33], extended with parameters for treating zeolite systems. The energy minimization scheme included an initial crude *steepest descents* step, followed by a *conjugated gradients* optimization, and was considered converged when the maximum derivative was less than 0.01 kcal mol^{-1} Å^{-1}.

3.2. Location and energetics of intermediates

In the literature, two different approaches are described for determining the location and energetics of organic molecules in porous solids. The first one is the docking procedure proposed by Freeman et al. [34], which starts with a high-temperature (e.g., 1500 K) molecular dynamics (MD) simulation of the isolated molecule. A certain number of conformations are randomly extracted from the MD trajectory and stored in an archive file for the subsequent Monte Carlo docking in the zeolite porous structure. After collection of the desired number of crudely docked structures, their energy optimization is performed.

The second approach involves the calculation of the adsorption enthalpy through the application of a Monte Carlo

technique [26]. In this case, both the zeolite framework and the organic molecule are kept fixed during the calculation.

In the case of bulky and flexible molecules (as the 1,1-diarylmethane intermediates) both these approaches generally fail because few of the possible conformations fit the porous structure. For this reason, we preferred to use a different procedure based on the quenched dynamics (QD) protocol [35], which was successfully applied for locating even complex organic molecules trapped within the pores during zeolite synthesis [36].

The QD protocol is a combination of constrained high-temperature molecular dynamics (MD) and energy minimization (EM) techniques. After building the zeolite model (a supercell with $P1$ symmetry is used and periodic boundary conditions are applied), the intermediate molecule was manually docked in the pores with a random orientation with respect to the framework. Its energy and orientation were optimized before starting the high-temperature MD simulation. To assure thorough exploration of the conformational space, to overpass all energy barriers between different conformers, and to allow molecular translations within the pores, the MD simulations were performed at 2000 K for 50 ps, with a 1-fs step (in the canonical NVT ensemble, with a constant number of particles, volume, and temperature). Every 500 fs, the MD simulation was interrupted and the resulting conformation was energy-minimized and archived for later elaboration. In case the molecule movements were limited to the neighborhood of its starting position, it was necessary to repeat the simulation with a different initial orientation of the molecule with respect to the framework.

For each intermediate/zeolite system, the minimum energy conformation was selected, further optimized, and considered converged when the maximum derivative was less than 0.001 kcal mol^{-1} Å^{-1}. All simulations were performed with the modules contained in the MSI Cerius^2 software package (release 4.2MS) [37].

The minimized energy was referred to that of the isolated intermediate and zeolite systems

$$E = E_{\text{intermediate/zeolite}} - E_{\text{intermediate}} - E_{\text{zeolite}}.$$

3.3. Approximations

All simulations were performed through the application of some approximations necessary for reducing the otherwise prohibitive computational efforts, incompatible with the aim of the work, i.e., the *a priori* selection of potential zeolite catalysts for the synthesis of 2,6-DMN.

3.3.1. Purely siliceous framework structures

The alkylation and isomerization reactions are acid-catalyzed, requiring the presence of Brønsted acid sites generated by the framework aluminum atoms. With few exceptions, all the structures considered are high-silica zeolites, containing only a few Al atoms per unit cell. In a first approximation, they are homogeneously distributed over all the crystallographically independent T-sites. Under the practical point of view, this situation is impossible to reproduce in models with a tractable number of atoms. Therefore, the simulations were performed on purely siliceous structures. This approximation is acceptable if one takes into account that the presence of the acid protons does not modify significantly the accessible space within the pores and, therefore, does not influence the definition of the MEP.

3.3.2. Neglect of electrostatic interactions

The simulations were performed after eliminating the electrostatic contribution to the potential energy. Though formally not correct, this approximation is acceptable since we are in the presence of low-polarity molecules, which experience the largely uniform electrostatic field of the purely siliceous structures [38].

3.3.3. Fixed framework

This is probably the most critical approximation because all phenomena related to the thermal vibration and to the relaxation of the structural modifications induced by the *guest* molecules are neglected. The first one is a dynamic phenomenon, which depends on the temperature and induces a fluctuation of the pore openings (*pore-breathing motion* [39]) of some one-tenth of Å around the equilibrium value. This may influence the diffusion of the molecules. In reality, the thermal vibrations occur on a time scale similar to that of the molecular vibrations ($\approx 10^{-13}$ s), while the diffusion of relatively large molecules (such as NAPH, NM, and DMN) is some order of magnitude slower. Therefore, during their diffusion, these molecules experience a fixed framework, with the crystallographically determined geometry, and the approximation can be considered acceptable. More critical is the second phenomenon, due to the fact that the *guest* molecule induces a relaxation into the framework to reduce the repulsive contribution to the nonbonding energy. However, the limited flexibility of the zeolite framework restricts the magnitude of this effect and the fixed framework approximation provides reasonably accurate values for the energy barriers. Therefore, this approximation is formally not correct but necessary for reducing the required computational time, while maintaining the meaning of the results.

3.4. Guest molecules

Fig. 4 shows the molecules selected for the MEP calculations. They include NAPH, the two methylnaphthalene isomers (1- and 2-MN), and four of the ten DMN isomers, representative of all possible steric situations present.

The quenched dynamics protocol was applied to the intermediate molecules shown in Fig. 5.

3.5. Zeolite structures

The zeolites used in the simulations were selected by considering the following criteria:

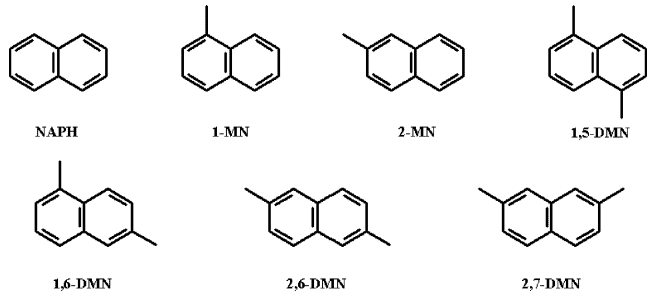

Fig. 4. Molecules used in the simulations of MEPs.

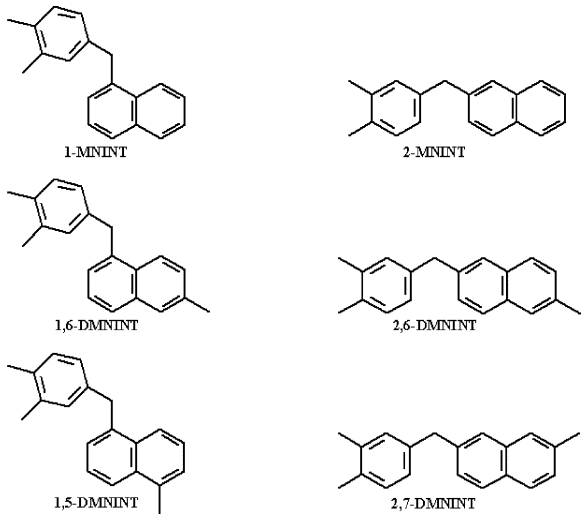

Fig. 5. 1,1-Diarylmethane intermediate molecules.

- pore dimensions sufficiently large to allow good diffusivity of the desired product;
- easy synthesis procedures or availability;
- possibility to modify their composition and morphology.

On the basis of the first criterion, the *small-pore* zeolites were obviously excluded since even NAPH (the less hindered molecule) is not able to diffuse in the 8-membered ring channels.

In the *medium-pore* zeolite class, the structural models of MFI [40] and EUO [41] were selected, while MOR [42], *BEA [43], FAU [44], MAZ [45], LTL [46], OFF [47], and MTW [48] were chosen among the *large-pore* structures. Within all these frameworks, the MEPs for all molecules listed in Fig. 4 were determined. Moreover, the location and energetics of the intermediate molecules shown in Fig. 5 were determined only for some of the selected structures (i.e., those effectively used in the catalytic tests).

4. Results and discussion

4.1. Determination of MEPs

The typical results obtained from the application of the forced diffusion procedure are exemplified in Figs. 6 and 7, where the snapshots for the diffusion of NAPH in MFI and MOR are reported, respectively, together with the corresponding energy plots (MEPs). These results can be interpreted as follows. Upon diffusing along the 10-MR linear channels of MFI and the 12-MR channels of MOR, the NAPH molecule potential energy depends on the local structure of the zeolite framework. The energy barriers (ΔE, a rough estimation of the activation energy of the diffusion process) encountered by the molecule during its diffusion are derived from the energy plots (Figs. 6 and 7). From the comparison between the MEP values and the corresponding snapshots, the barrier-determining environments are easily identifiable. The simulation results are summarized in Table 2.

4.1.1. Medium-pore zeolites

According to the observed ΔE values, the diffusion of all molecules in MFI and EUO is predicted to be rather difficult or even, in the case of the isomers with at least a $-CH_3$ group in the α-position (1-MN, 1,5-DMN, and 1,6-DMN), impossible (Table 2 and Fig. 8). The ΔE values for NAPH in MFI and EUO are almost identical (Table 2) while the energy barriers for the diffusion of the two desired products (2-MN and 2,6-DMN) are significantly lower in the case of EUO (Table 2). Another interesting observation deals with the ΔE values for the 2,7-DMN isomer which, in both zeolites, are predicted to be larger than those for 2,6-DMN (Table 2). Therefore, it is possible to hypothesize that MFI and EUO display *product shape-selectivity* properties with respect to the 2,7-DMN isomer.

The obtained results indicate *medium-pore* zeolites as potential catalysts for the alkylation reaction of NAPH with methanol, while they exclude the use of these materials for the isomerization of 1-MN and of DMN isomers with methyl groups in α-positions. Actually, very high energy barriers hamper both adsorption and diffusion of these molecules. Between the two examined *medium-pore* zeolites, EUO seems preferable because of the lower ΔE values that characterize the MEPs of 2-MN and 2,6-DMN.

4.1.2. Large-pore zeolites

Examination of the data reported in Table 2 and in Fig. 9 indicates that the diffusivity of the molecules in the investigated porous systems decreases in the order

$$\text{NAPH} \approx \text{2-MN} \approx \text{2,6-DMN} > \text{2,7-DMN} > \text{1-MN} \approx \text{1,6-DMN} > \text{1,5-DMN}.$$

This agrees with their relative steric hindrance.

NAPH, 2-MN, 2,6-DMN, and 2,7-DMN are predicted to diffuse substantially unhindered in all simulated structures ($\Delta E_{\max} \approx 28\ \text{kJ mol}^{-1}$, Table 2), with the exception of the latter in MTW, which displays the highest energy barriers ($\Delta E_{\max} \approx 102.6\ \text{kJ mol}^{-1}$, Table 2). All other molecules, i.e., those containing at least a methyl group in the α-position, behave differently, depending on the size and

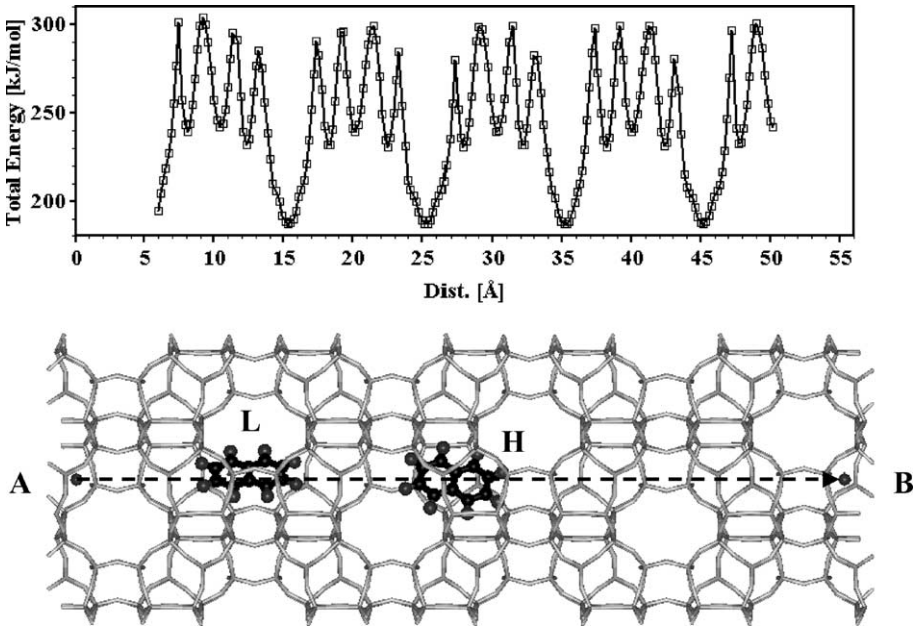

Fig. 6. MEP for NAPH in the straight 10MR channel of MFI. A and B define the starting and end points of the trajectory; the lowest and highest energy conformation of the NAPH molecule are indicated by L and H, respectively.

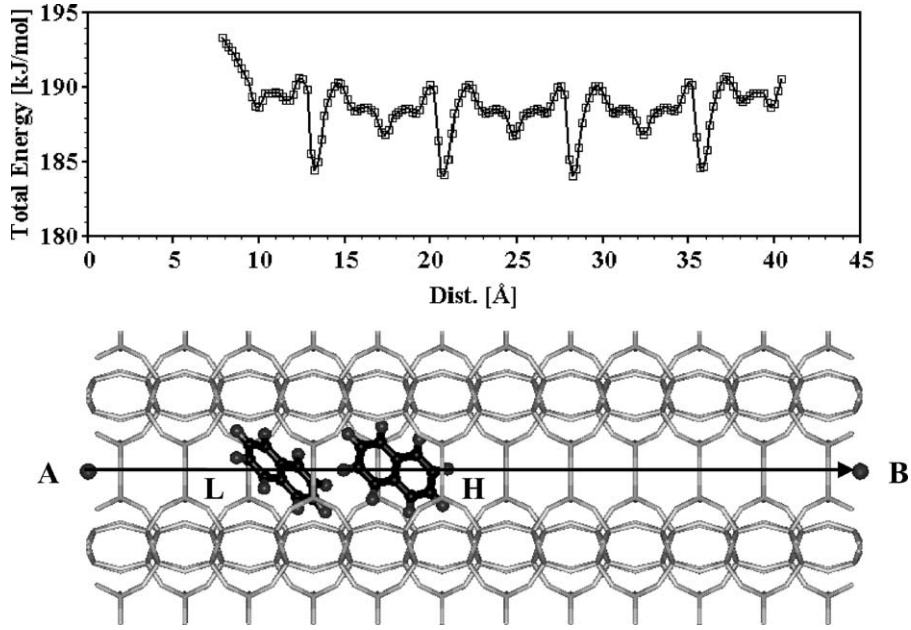

Fig. 7. MEP for NAPH in the straight 12MR channel of MOR. A and B define the starting and end points of the trajectory; the lowest and highest energy conformation of the NAPH molecule are indicated by L and H, respectively.

shape of the pores (Table 2). In fact, the energy barriers increase as the pore dimensions decrease: the simulations predicted that these molecules easily diffuse only in MOR, *BEA, FAU, MAZ, and LTL (the zeolites with the largest pore size). On the other hand, in OFF and MTW too large energy barriers exist for considering free displacements along the pores. In the case of MTW, the evaluation of the MEPs for 1,5-DMN and 1,6-DMN failed since these molecules remained fixed to their starting positions, even after imposing a high pushing potential of 400 kJ mol^{-1}. This behavior is surprising when considering that it was possible to determine the energy barriers for the diffusion of the same DMN isomers in MFI and EUO, whose linear channels are characterized by free dimensions slightly smaller than those of MTW (Table 2). However, MFI and EUO porous systems are characterized by the presence of large voids (intersections between the two 10MR channel systems and large side pockets, respectively), which allow the calculation of the MEPs for the two DMN isomers, even if with very high energy barriers. In contrast, the lack of large voids and the relatively

Table 2
Energy barriers for the diffusion of all molecules in the selected zeolites (data in kJ mol^{-1})

Zeolite	Pore size (Å)[a]	NAPH	1-MN	2-MN	1,5-DMN	1,6-DMN	2,6-DMN	2,7-DMN
				Medium-pore zeolites				
MFI	[010] **10** 5.3 × 5.6	114.2	450.4	217.7	747.6	456.2	202.1	276.0
EUO	[100] **10** 4.1 × 5.7	113.8	295.9	182.1	282.6	257.9	106.8	159.0
				Large-pore zeolites				
MOR	[001] **12** 6.5 × 7.0	7.1	12.2	5.9	12.1	10.8	4.5	5.1
MAZ	[001] **12** 7.4	8.6	16.7	8.4	22.1	17.8	7.1	7.5
*BEA	[001] **12** 6.4 × 7.6	13.8	19.3	19.3	34.7	30.1	8.1	14.3
FAU	⟨111⟩ **12** 7.4	8.7	34.3	18.3	34.3	38.9	21.3	23.3
LTL	[001] **12** 7.1	27.7	61.1	21.8	36.4	39.4	14.6	28.7
OFF	[001] **12** 6.7	27.6	88.7	25.8	72.6	54.6	24.7	18.8
MTW	[010] **12** 5.5 × 5.9	11.7	55.8	11.3	No diff.	No diff.	10.9	102.6

[a] Free dimensions of the channels in which the MEPs were simulated.

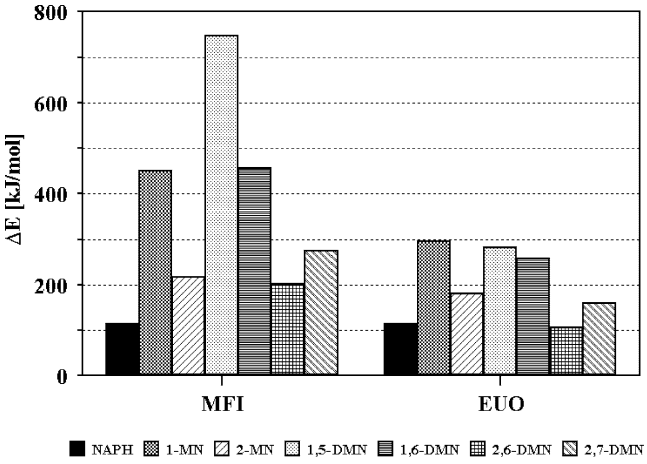

Fig. 8. Energy barriers computed for all molecules in the *medium-pore* zeolites.

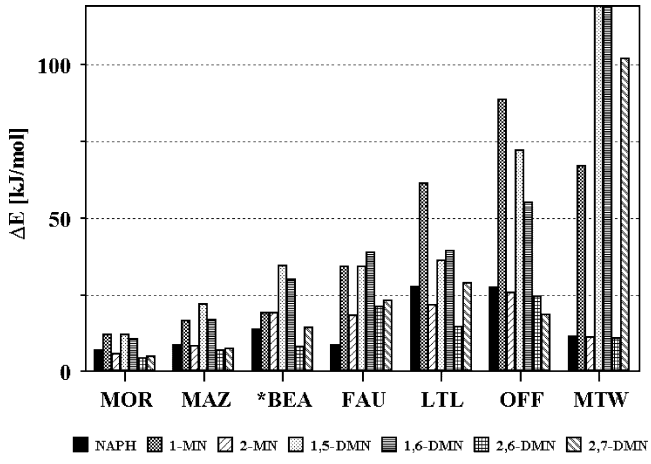

Fig. 9. Energy barriers computed for all molecules in the *large-pore* zeolites.

small free dimensions of the pores hamper the diffusion of 1,5- and 1,6-DMN in MTW.

From these results, it is possible to conclude that MOR, *BEA, MAZ, and FAU can potentially be used for the isomerization reaction. In fact, the low-energy barriers for 1-MN, 1,5-DMN, and 1,6-DMN make the adsorption and the diffusion of these molecules possible, while the formation of the desired products (2-MN and 2,6-DMN) is favored by their higher thermodynamic stability. Because of their expected low selectivity, the same zeolites seem to be less favorable for the alkylation of NAPH and 2-MN with methanol. As far as the other zeolite structures are concerned, the simulations indicate that they are more suitable for the alkylation reaction, where a relatively high selectivity toward the β-methyl isomers is expected. As a matter of fact, the adsorption and diffusion of the α-methyl-substituted naphthalenes is predicted to be difficult if not impossible (Table 2).

Another important point concerns the undesired 2,7-DMN isomer. From the thermodynamic point of view, 2,6-DMN and 2,7-DMN share the same stability; therefore, the only way to limit the formation of the undesired isomer is to exploit the *product shape-selectivity* properties of a suitable microporous catalyst. In almost all the examined zeolites, the ΔE values computed for these isomers are very similar and the observed differences are not sufficiently high to predict relevant selectivity toward the two products. The only case where significant differences have been observed is MTW. In fact, 2,6-DMN is predicted to diffuse substantially unhindered in the puckered 12-MR channels, while the 2,7-DMN is not ($\Delta E = 10.9$ and 102.6 kJ mol^{-1}, respectively, Table 2).

4.2. Catalytic tests: comparison with modeling results

Table 2 shows the results of the catalytic tests performed on selected *medium-* and *large-pore* zeolites in the presence of pseudocumene (1,2,4-trimethylbenzene, TMB) as a solvent [20]. *Medium-pore* zeolites (MFI and EUO) exhibited lower activity with respect to *large-pore* structures [20]. MFI is more active and selective than EUO, even if it forms ethylnaphthalenes (ENs) as by-products (Table 3). It must be pointed out that all considered molecules can be easily hosted both in the MFI intersections of two 10MR channel systems and in the EUO large lateral pockets. However, even if allowed to form, their diffusion is predicted to be quite

Table 3
Catalysts screening tests (623 K, 4 MPa, WHSV 0.86 h^{-1}, TMB:NAPH:MeOH = 10:1:3) [20]

	MFI	EUO	MOR	MAZ	Beta		FAU		MTW
SiO_2/Al_2O_3 ratio	30	30	20	8	24		6		100
t.o.s. (h)	7	10	15	32	28	95	24	95	95.5
NAPH conv. (%)	19.5	12.8	20.8	23.1	53.7	26.1	47.7	21.7	50.8
Selectivity									
MNs	57.1	86.3	79.2	82.7	61.3	77.5	65.6	84.1	64.6
DMNs	18.5	10.2	11.9	15.2	27.0	9.9	24.7	14.8	32.5
2,6-DMN	4.0	2.0	2.4	1.1	4.4	2.5	3.6	1.4	9.0
Σ2,6-DMN[a]	6.2	4.1	5.8	3.8	10.1	4.8	7.8	3.9	18.6
PMNs[b]	4.3	3.5	4.6	2.0	11.7	12.6	9.7	1.1	2.9
ENs[c]	20.0	0	0	0	0	0	0	0	0
2,6-DMN/DMNs	21.5	19.1	20.0	7.0	16.2	25.6	14.7	9.7	27.5
Σ2,6-DMN/DMNs	33.6	40.3	49.3	24.7	37.5	48.9	31.5	26.5	57.2
2,6-/2,7-DMN	0.5	1.1	1.5	1.2	1.2	1.3	1.1	1.1	2.0

[a] Σ2,6-DMN = sum of 2,6-/1,6-/1,5-DMN as they belong to the same isomerization group [13].
[b] PMNs = naphthalenes bearing three or more methyl groups.
[c] ENs = ethylnaphthalenes.

difficult on the basis of the height of the energy barriers characterizing their MEPs (Table 2). Nonetheless, the ΔE values predicted for EUO are significantly smaller than those computed for MFI and that result contrasts somewhat with the product distributions observed in the catalytic tests (Table 3). In particular, the expected increase of the 2,6-/2,7-DMN ratio with respect to the equilibrium value was not observed and the formation of relatively high amounts of PMNs even contrasts with the simulation results.

More interesting results were obtained with the *large-pore* zeolites. In particular, among the tested structures, only Beta, FAU, and MTW exhibited useful activities, while MOR and MAZ were less active (Table 3) [20]. To compare Beta, FAU, and MTW in greater detail, additional data (at similar NAPH conversion) are reported in Table 3 for the first two catalysts. In all cases MTW displayed the best performances, with high selectivity to 2,6-DMN and to Σ2,6-DMN (9.0 and 18.6, respectively, Table 3). Most interesting is the experimental 2,6-/2,7-DMN ratio of 2.0 observed in the case of MTW, well above the thermodynamic value. This is in fair agreement with the large difference between the calculated ΔE values of the two isomers (10.9 and 102.6 kJ mol^{-1} for 2,6- and 2,7-DMN, respectively, Table 2). It is interesting to note that the 2,6-/2,7-DMN ratio can be increased to 2.5–2.6 when MNs are used as feed [20]. These two isomers are predicted to diffuse practically unhindered in all other *large-pore* zeolite structures and, in those cases, the experimental ratio was found in the range 1.1–1.5 (Table 3). Another interesting feature derived from the simulations with the MTW structure is the difficult (if not impossible) diffusion of the DMN isomers bearing a methyl group in the α-position (Table 2).

4.3. Location and energetics of intermediate molecules

The QD protocol we adopted proved to be suitable for determining the location and energetics of the intermediate molecules. As an example, the results obtained in the simulation of the 2,6-DMNINT molecule in MTW are shown in Fig. 10. One hundred different conformations were extracted from the MD trajectory and energy minimized. They were considered enough for the exploration of the linear 12-membered ring channel of MTW. As shown in the total energy plot, several minima were found together with other less stable conformations.

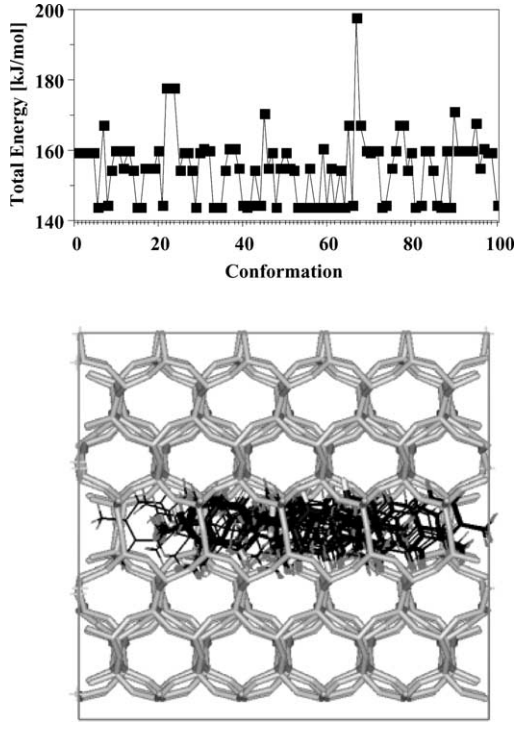

Fig. 10. Search for the low-energy site for the adsorption of 2,6-DMNINT in MTW.

The same situation was found for all the *large-pore* zeolites as well as for EUO while in the case of MFI two or more different QD runs were necessary for finding the lowest energy location of the molecules.

Table 4
Valence, van der Waals, and total energy values of intermediate molecules in the different zeolites (data in kJ mol^{-1})

Zeolite		1-MNINT	2-MNINT	2,6-DMNINT	2,7-DMNINT	1,6-DMNINT	1,5-DMNINT
				Medium-pore zeolites			
MFI	Valence	70.2	34.3	34.7	33.5	70.2	149.6
	vdW	−151.7	−203.1	−222.8	−223.0	−175.0	−179.6
	Total	−81.5	−168.8	−188.1	−189.5	−104.8	−30.0
EUO	Valence	4.9	17.0	16.3	21.8	22.1	30.0
	vdW	−269.6	−259.2	−266.9	−293.2	−270.9	−235.1
	Total	−264.7	−242.2	−250.6	−271.4	−269.8	−205.1
				Large-pore zolites			
*BEA	Valence	9.4	5.7	5.7	1.6	9.4	9.8
	vdW	−240.7	−244.2	−259.2	−258.4	−250.5	−246.8
	Total	−231.3	−238.5	−253.5	−256.8	−241.1	−237.0
MOR	Valence	5.0	2.7	5.6	4.7	5.1	6.5
	vdW	−233.3	−267.4	−284.3	−284.2	−250.4	−245.1
	Total	−228.3	−264.7	−278.7	−279.5	−245.3	−238.6
MAZ	Valence	2.1	0.1	0.2	0.8	2.8	1.9
	vdW	−224.9	−240.7	−257.6	−254.3	−237.4	−241.2
	Total	−222.7	−240.6	−257.4	−253.5	−234.6	−239.3
FAU	Valence	1.2	1.1	1.2	1.2	2.5	0.5
	vdW	−185.8	−181.7	−192.2	−192.2	−194.9	−193.4
	Total	−184.6	−180.6	−191.0	−191.0	−192.4	−192.9
MTW	Valence	47.3	21.0	20.7	19.8	46.9	47.1
	vdW	−241.5	−277.6	−298.1	−297.7	−261.8	−235.6
	Total	−194.1	−256.6	−277.4	−277.9	−214.9	−208.5

The overall results are listed in Table 4. For each intermediate/zeolite system, the valence (i.e., the sum of the bond lengths, bond angle, torsion angle, out-of-plane deformation, and cross-term energy contributions), nonbonded (i.e., the van der Waals energy only since electrostatic interactions were neglected), and total energy (i.e., the sum of the valence and nonbonded energy contributions) are reported. The inspection of the two components of the total energy of the systems is useful for better understanding the different situations experienced by the intermediate molecules in the different porous structures. The valence energy is a measure of the strain imposed to the molecule by the framework, while the van der Waals energy gives an indication of the steric compatibility of the molecule itself while docked in the porous structure.

The valence energy significantly varies from one structure to another: as expected, the restricted MFI porous structure imposes a significant strain on all intermediate molecules, which becomes particularly high for 1-MNINT, 1,6-DMNINT, and 1,5-DMNINT (Table 4). The same is not true in the case of EUO, the other *medium-pore* zeolite considered, because of the presence of the large side pockets, which assure enough space for hosting the intermediate molecules with relatively limited strain. The strain energy of the molecules is compensated by favorable nonbonded interactions with the zeolite framework, which finally lead to an overall stabilization of the system, more pronounced for EUO than for MFI (Table 4). Upon considering the total energy of the systems, it appears clear that in MFI the formation of 1-MNINT, 1,6-DMNINT, and 1,5-DMNINT is less favored with respect to the other intermediate molecules. This fact led us to the conclusion that the formation of 2-MN, 2,6-DMN, and 2,7-DMN is favored by transition state shape selectivity. However, because of the high-energy barriers hampering their diffusion (Fig. 8), these molecules may undergo further reactions before being eluted, with the formation of ENs (Table 3) or polyalkylated molecules, which lead to the fast deactivation of the catalyst.

With the exception of 1,5-DMNINT, no significant differences exist among the total energy values of the intermediate molecules in EUO. That means that this zeolite is not characterized by transition state shape-selective properties. Again, the relatively high ΔE values which characterize the MEPs of the products may be responsible for the fast deactivation of the catalyst (Fig. 8).

In the case of the *large-pore* zeolites, with the exception of MTW, the valence energy of all intermediate molecules is very low, close to that of the isolated molecules (Table 4). Some difference is however observed for the van der Waals energy. In particular, in the case of FAU (the zeolite with the largest pore volume) the total energy is practically the same for all molecules (Table 4), in agreement with the presence of large supercages in which the intermediate molecules can be freely located. Therefore, FAU should be considered as completely nonselective. The same considerations are valid for MAZ and *BEA but not for MOR, for which small but clear preferences toward 2-MNINT, 2,6-DMNINT, and 2,7-DMNINT are predicted (Table 4).

In the case of MTW, in contrast, we observe that 1-MNINT, 1,6-DMNINT, and 1,5-DMNINT are significantly more strained and their interaction with the framework less favorable with respect to the other intermediate molecules

(Table 4). In the puckered 12-membered ring channels of MTW, 2-MNINT, 2,6-DMNINT, and 2,7-DMNINT are better stabilized than the other molecules. This leads to the conclusion that, among the examined *large-pore* zeolites, MTW is the only one which displays useful transition state shape selectivity. The last observation concerns 2,6- and 2,7-DMN: according to the data reported in Table 4, the corresponding intermediate molecules display the same energy and their formation is predicted to have the same probability. The high 2,6-/2,7-DMN ratio observed in the product can be justified with the large difference in the ΔE values, and hence in the diffusion behavior, of the two molecules (Fig. 9).

5. Conclusions

Molecular mechanics calculations of the minimum energy pathway for diffusion of MNs and DMNs isomers were used to select potential zeolite catalysts for the synthesis of 2,6-DMN through the alkylation of NAPH with methanol and/or isomerization of DMN isomers. In particular, the MEP for the diffusion of reactants and products in the porous systems of selected *medium*- and *large-pore* zeolites was determined. From that the height of the energy barriers was derived, which is in a first approximation related to the activation energy of the diffusion process. Inspection of the obtained results led to the following conclusions.

- The diffusion of NAPH, MNs, and DMNs in *medium-pore* MFI and EUO zeolites is rather difficult; this is particularly true for the isomers bearing a $-CH_3$ group in the α-position, suggesting that these zeolites would not be useful in the isomerization reaction of DMNs. The simulations predicted EUO as a more suitable catalyst with respect to MFI, but the reduced pore size of both zeolites may favor their rapid deactivation, as demonstrated by the catalytic tests.
- The situation in the case of the *large-pore* zeolites is more complex. NAPH, 2-MN, 2,6-DMN, and with the exception of MTW, 2,7-DMN can easily diffuse in all examined structures. In contrast, significant differences are predicted among the diffusivities of the molecules bearing a methyl group in the α-position. For the MOR, MAZ, *BEA, and FAU zeolites an easy diffusion of all molecules is predicted; therefore, these structures should be considered suitable for the isomerization but not for the alkylation reaction. An opposite situation is predicted for MTW where strong restrictions exist to the diffusion of 1-MN, 1,5-DMN, and 1,6-DMN. Furthermore, a 2,6-/2,7-DMN ratio significantly larger than that expected on a purely thermodynamic basis can be predicted for MTW. An intermediate situation was observed for LTL and OFF.

Catalytic tests confirmed the predictions and indicated MTW as the best catalyst for the alkylation of NAPH to 2,6-DMN, with a 2,6-/2,7-DMN ratio in the range 2.0–2.6. These results confirm that the modeling tools may provide useful information for choosing suitable zeolite catalyst for the selective synthesis of 2,6-DMN.

Since the reaction was performed in the presence of TMB as a solvent, the good catalytic performances of MTW can be justified by taking into account also the formation probability of 1,1-diarylmethane intermediate molecules. They derive from the electrophilic attack of a benzyl carbocation to the naphthalene or methylnaphthalene ring. Unique among the examined *large-pore* zeolites, MTW showed a larger stabilization of the molecules involved in the formation of 2-MN, 2,6-DMN, and 2,7-DMN. Such products can be considered more likely to form than those bearing at least a $-CH_3$ group in the α-position.

References

[1] L.D. Lillwitz, Appl. Catal. 221 (2001) 337.
[2] T. Abe, S. Uchiyama, T. Ojima, K. Kida, US 5,008,479, 1991, assigned to MGC.
[3] T. Abe, S. Uchiyama, S. Machida, K. Kida, US 5,023,390, 1991, assigned to MGC.
[4] K. Taniguchi, S. Miyamoto, H. Matsuoka, US 3,931,348, 1976, assigned to Mitsui.
[5] K. Vahteristo, E. Halme, S. Koskimies, S.M. Csicsery, M. Laatikainen, V. Niemi, WO 97/02225, 1997, assigned to Optatech Corp.
[6] D. Fraenkel, M. Cherniavsky, B. Ittah, M. Levy, J. Catal. 101 (1986) 273.
[7] J. Weitkamp, M. Neuber, Stud. Surf. Sci. Catal. 6 (1990) 291.
[8] E. Kikuchi, Y. Mogi, T. Matsuda, Coll. Czech. Chem. Commun. 57 (1992) 909.
[9] T. Komatsu, Y. Araki, S. Namba, T. Yashima, Stud. Surf. Sci. Catal. 84 (1994) 1821.
[10] Z. Popova, M. Yankov, L. Dimitrov, Stud. Surf. Sci. Catal. 84 (1994) 1829.
[11] A.S. Loktev, P.S. Chekruy, Stud. Surf. Sci. Catal. 84 (1994) 1845.
[12] S.-B. Pu, T. Inui, Appl. Catal. A: General 146 (1996) 305.
[13] S.-B. Pu, T. Inui, Zeolites 17 (1996) 34.
[14] O.A. Anunziata, L.B. Pierella, Catal. Lett. 44 (1997) 259.
[15] S.J. Kulkarni, K.V.V.S.B.S.R. Murthy, K. Nagaiah, V. Sylesh Kumar, Y.V. Subba Rao, M. Subrahmanyam, A.V. Rama Rao, Indian J. Chem. Technol. 5 (1) (1998) 62.
[16] R. Gläser, R. Li, M. Hunger, S. Ernst, J. Weitkamp, Catal. Lett. 50 (1998) 141.
[17] K. Sumitani, K. Shimada, JP 413,637, 1992, assigned to Teijin.
[18] M. Motoyuki, K. Yamamoto, J. McWilliams, R. Bundens, US 5,744,670, 1998, assigned to Kobe-Mobil.
[19] P.J. Angevine, T.F. Degnan, D.O. Marler, US 5,001,295, 1991, assigned to Mobil.
[20] G. Pazzuconi, G. Terzoni, C. Perego, G. Bellussi, Stud. Surf. Sci. Catal. 135 (2001) 25-O-03.
[21] G. Pazzuconi, C. Perego, R. Millini, F. Frigerio, R. Mansani, D. Rancati, US 6,147,270, 2000, assigned to EniTecnologie–EniChem.
[22] J.A. Horsley, J.D. Fellmann, E.G. Derouane, C.M. Freeman, J. Catal. 147 (1994) 231.
[23] R. Millini, S. Rossini, Stud. Surf. Sci. Catal. 105 (1996) 1389.
[24] L. Domokos, L. Lefferts, K. Seshan, J.A. Lercher, J. Catal. 203 (2001) 351.
[25] C. Perego, S. Amarilli, R. Millini, G. Bellussi, G. Girotti, G. Terzoni, Micropor. Mater. 6 (1996) 395.

[26] P. Raybaud, A. Patrigeon, H. Toulhoat, J. Catal. 197 (2001) 98.
[27] R.C. Deka, R. Vetrivel, J. Catal. 174 (1998) 88.
[28] M. Sierka, J. Sauer, J. Chem. Phys. 112 (2000) 6983.
[29] G.A. Olah, A. Molnar, Hydrocarbon Chemistry, Wiley, New York, 1995.
[30] Catalysis, Release 4.0, Molecular Simulations, San Diego, CA, 1996.
[31] Discover, Molecular Simulations, San Diego, CA, 1996.
[32] J.-R. Hill, J. Sauer, J. Phys. Chem. 98 (1994) 1238.
[33] P. Dauber-Osguthorpe, V.A. Roberts, D.J. Osguthorpe, J. Wolff, M. Genest, A.T. Hagler, Proteins: Struct. Funct. Genet. 4 (1988) 31.
[34] C.M. Freeman, C.R.A. Catlow, J.M. Thomas, S. Brode, Chem. Phys. Lett. 186 (1991) 137.
[35] R. Millini, L.C. Carluccio, A. Carati, W.O. Parker Jr., Micropor. Mesopor. Mater. 46 (2001) 191.
[36] R. Millini, Stud. Surf. Sci. Catal. 135 (2001) 264.
[37] Cerius^2, Release 4.2MS, Molecular Simulations, San Diego, CA, 2000.
[38] D.W. Lewis, C.M. Freeman, C.R.A. Catlow, J. Phys. Chem. 99 (1992) 11194.
[39] M.W. Deem, J.M. Newsam, J.A. Creighton, J. Am. Chem. Soc. 114 (1992) 7198.
[40] H. van Koningsveld, H. van Bekkum, J.C. Jansen, Acta Crystallogr. B 43 (1987) 127.
[41] N.A. Briscoe, D.W. Johnson, M.D. Shannon, G.T. Kokotailo, L.B. McCusker, Zeolites 8 (1988) 74.
[42] A. Alberti, P. Davoli, G. Vezzalini, Z. Kristallogr. 175 (1986) 249.
[43] J.M. Newsam, M.M.J. Treacy, W.T. Koetsier, C.B. de Gruyter, Proc. R. Soc. (London) A 420 (1988) 375.
[44] J.A. Hriljac, M.M. Eddy, A.K. Cheetham, J.A. Donohue, G.J. Ray, J. Solid State Chem. 106 (1993) 66.
[45] E. Galli, Cryst. Struct. Commun. 3 (1974) 339.
[46] J.M. Newsam, J. Phys. Chem. 93 (1989) 7689.
[47] J.A. Gard, J.M. Tait, Acta Crystallogr. B 28 (1972) 825.
[48] C.A. Fyfe, H. Gies, G.T. Kokotailo, B. Marler, D.E. Cox, J. Phys. Chem. 94 (1990) 3718.